JPE 4-2-1

Static VAR Compensator-based Feedback Control Implementation for Self-Excited Induction Generator Terminal Voltage Regulation Driven by Variable-Speed Prime Mover

Tarek Ahmed†, Katsumi Nishida, and Mutsuo Nakaoka

The Graduate School of Science and Engineering, Yamaguchi University, Yamaguchi, Japan

ABSTRACT

In this paper, the steady-state analysis of the three-phase self-excited induction generator (SEIG) driven by a variable-speed prime mover (VSPM) such as a wind turbine is presented. The steady-state torque-speed characteristics of the VSPM are considered with the three-phase SEIG equivalent circuit for evaluating the operating performances due to the inductive load variations. Furthermore, a PI closed-loop feedback voltage regulation scheme based on the static VAR compensator (SVC) for the three-phase SEIG driven by the VSPM is designed and considered for the wind power generation conditioner. The simulation and experimental results prove the practical effectiveness of the additional SVC with the PI controller-based feedback loop in terms of fast response and high performances.

Keywords : Self-excited induction generator, Variable-speed wind turbine, Static VAR compensator, Voltage regulation

1. Introduction

The three-phase induction machine with a squirrel cage or wound rotor could work as a three-phase induction generator either connected to the utility ac power distribution line or operated in the self-excitation power generation mode with an additional excitation capacitor bank [1-3]. The terminal voltage and the output frequency of the three-phase induction generator are the same as the utility grid ac voltage and the commercial frequency of the utility ac power source to which the three-phase induction generator is connected[4-6].

Manuscript received May 20, 2003; revised Mar. 2, 2004.

† Corresponding Author: tarek@pe-news1.eee.yamaguchi-u.ac.jp
Tel: +81-836-85-9472, Fax: +81-836-85-9401

The reactive power required for the three-phase induction generator is to be supplied by the utility ac power source and the active output power of the three-phase induction generator is delivered to the utility ac power source. With the fixed frequency of the utility ac power source, the three-phase induction machine starts to operate in the generation mode when the rotor shaft speed is above the synchronous speed. The operating range of the rotor shaft speed is also limited by the slip of the three-phase induction machine[6-8]. In case of a high slip, the winding copper losses increase as the currents increase. On the other hand, in an isolated stand-alone operation for clean alternative renewable energy utilizations, the three-phase induction generator operates in the self-excitation power generation mode when an appropriate capacitor bank connected in parallel with its stator terminal ports and driven by a renewable energy prime

mover as wind turbine energy [9-11]. The three-phase self-excited induction generator (SEIG) determines its own generated terminal voltage and its output frequency, which depend on the capacitance of the excitation capacitor bank, the three-phase induction machine parameters, the inductive load components, and the speed of the prime mover[12-16].

Over the past decade years, few researchers have attempted to analyze the steady-state and dynamic performances of the three-phase SEIG driven by a constant-speed prime mover[5-12]. The possible and effective applications of the three-phase SEIG driven by a variable-speed prime mover such as a wind turbine for stand-alone applications are currently under investigation [13-16]. The generated output voltage can be directly connected to the load facility installation and equipment are non-sensitive to the ac frequency such as an electric heater or to a battery charger using a diode rectifier circuit.

This paper describes an effective algorithm for evaluating the steady-state performance analysis of the three-phase SEIG driven by a variable-speed prime mover (VSPM) for a stand-alone power supply. In addition, the simulation and experimental results of the PI closed-loop feedback using the static VAR compensator (SVC) composed of the thyristor controlled reactor (TCR), the thyristor switched capacitor (TSC) and the fixed excitation capacitor bank (FC) for the terminal voltage regulation of the three-phase SEIG driven directly by the VSPM are established and discussed in this paper.

2. System Configuration

The schematic system diagram of the three-phase SEIG voltage regulation based on the SVC controlled by a PI controller in the feedback loop is shown in Fig. 1. The 4 poles, 220 V, 2 kW squirrel cage three-phase SEIG with star connected stator winding is designed for supplying a balanced three-phase inductive load. The three-phase SEIG is excited by the SVC composed of the FC, the TSC and the TCR, which is based on the synchronous phase angle control strategy. The thyristor triggering circuit per-phase for the TCR and the PI controller circuit in a feedback control scheme are designed and shown in Fig.2 and Fig. 3, respectively. Table 1 indicates the design specifications and the induction machine parameters of three-phase SEIG and the constant circuit parameters of the voltage regulation system for the three-phase SEIG with the SVC operated by the PI compensator.

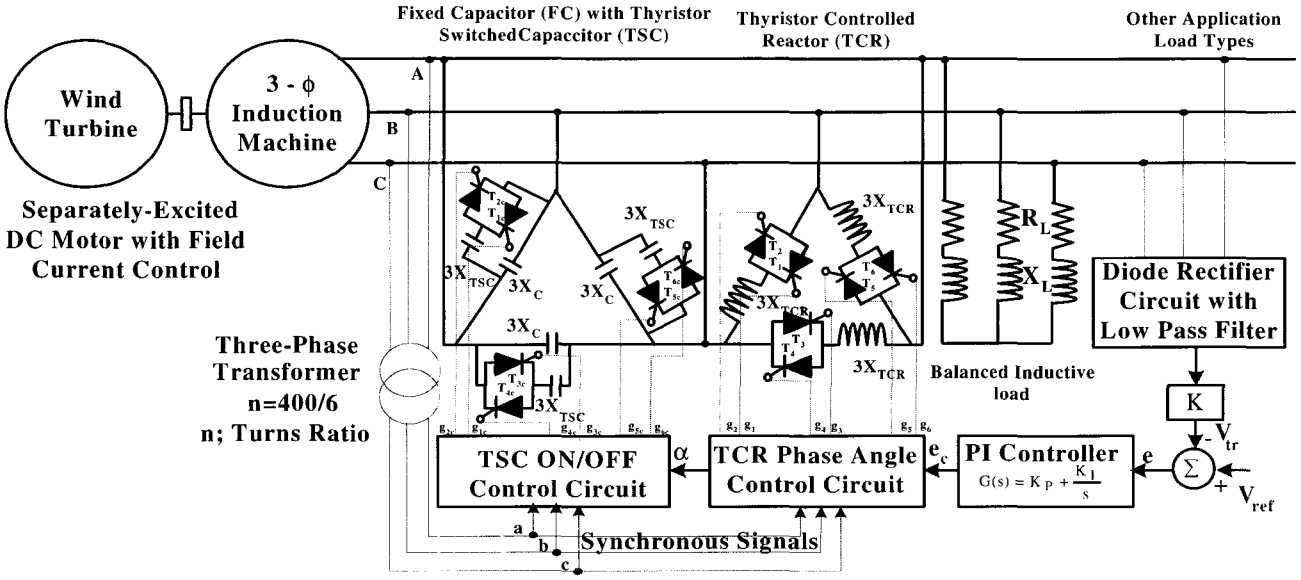

Fig. 1. A schematic system configuration of VSPM coupled three-phase SEIG with SVC including PI controller.

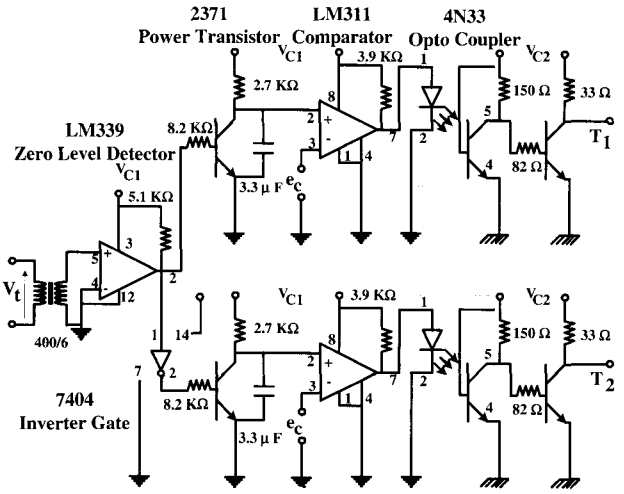

Fig. 2. Designed thyristors triggering circuit per-phase for TCR.

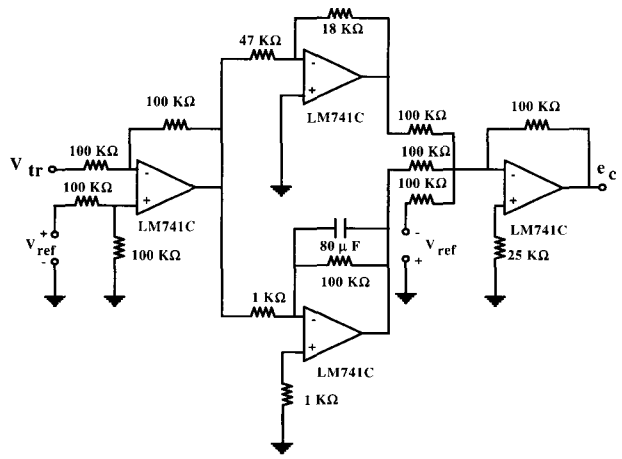

Fig. 3. Designed PI controller circuit.

Table 1. Design Specifications and Circuit Parameters.

Items	*Machine Rating and Machine Parameters*	
Three-Phase Star Connected Induction Machine with Squirrel Cage Rotor	Rated Voltage	220 V
	Rated Power	2 kW
	Number of Poles	4
	Induction Machine Parameters at 50 Hz	
	R_1=0.517 ohm	X_1=1.0063 ohm
	R_2=0.517 ohm	X_2=1.0063 ohm
SVC composed of FC, TCR &TSC	X_{TCR} at 50 Hz; L_{TCR}	20 ohm, 0.064 H
	X_C at 50 Hz; C	13 ohm, 244 μF
	X_{TSC} at 50 Hz; C_{TSC}	64 ohm, 50 μF
PI Controller	K_P	0.38
	K_I	12.5
Low Pass Filter	C_{LPF}	2000 μF
VSPM (dc Motor)	τ_o	See Fig.4
	υ_o	See Fig.4
Per-Phase Inductive Load Components	R_L	35-200 ohm
	X_L at 50 Hz	25-140 ohm

3. Variable-Speed Prime Mover Characteristics

The mechanical output power P_m of the VSPM is defined as [1]-[2],

$$P_m = T_m \omega_s \upsilon \tag{1}$$

where $\upsilon(\upsilon=N/N_s)$ is the per unit speed of the VSPM. N and N_s are the rotor speed and the three-phase SEIG rated synchronous speed in rpm, respectively. $\omega_s(\omega_s=2\pi N_s/60)$ is the rated synchronous angular speed. T_m is the mechanical output torque of the VSPM in N.m and can be represented by,

$$T_m = \tau_o - \upsilon_o \upsilon \tag{2}$$

where τ_o and υ_o respectively are the coefficients of the torque-speed characteristics in N.m.

In experiment, a controllable separately-excited dc motor is used with a constant armature voltage and a field current control. Fig. 4 illustrates the effect of the field current control on the torque-speed characteristics and the corresponding torque-speed coefficients τ_o and υ_o which are given by,

$$\tau_o = \frac{K_t \phi_m V_a}{R_a} \quad \text{and} \quad \upsilon_o = \frac{2\pi K_t^2 \phi_m^2}{60 R_a} N_s$$

where K_t, ϕ_m, V_a and R_a are the torque constant, the field flux per pole in wb, the armature voltage in Volt and the armature resistance in Ohm of the dc motor, respectively.

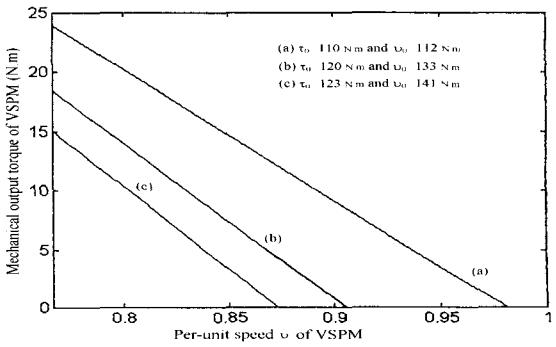

Fig. 4. Torque-speed characteristics of VSPM.

4. SVC with PI Compensator For Three-Phase SEIG Voltage Regulation

The instantaneous inductive current flowing through the inductor of TCR shown in Fig.1 with the thyristor triggering delay angle α is expressed by [2]-[3],

$$i_{TCR}(t)=\begin{cases}\dfrac{\sqrt{2}V_t}{X_{TCR}}(\cos\alpha-\cos\omega t) & \alpha\le\omega t\le\alpha+\sigma\\ 0 & \sigma+\alpha\le\omega t\le\alpha+\pi\end{cases} \quad (3)$$

where α is the thyristor triggering delay angle with respect to the zero crossing output voltage waveform, σ is the conduction angle of the thyristor, X_{TCR} is the equivalent inductive reactance of the TCR inductor. V_t is the per-phase effective value of the three-phase SEIG generated output voltage and ω is the electrical angular frequency. With neglecting the harmonic currents generated by the switched inductances, the fundamental component of the TCR inductive current is obtained on the basis of using the Fourier series expansion as follows,

$$I_{TCR1}=B_{TCR}(\sigma)V_t \quad (4)$$

where $B_{TCR}(\sigma)$ is the equivalent inductive susceptance of the TCR and defined a function of the conduction angle σ as[3],

$$B_{TCR}(\sigma)=\frac{\sigma-\sin(\sigma)}{\pi X_{TCR}} \quad (5)$$

The relationship between the conduction angle σ and the thyristor triggering delay angle α of the TCR is given by[3],

$$\text{where}\quad \alpha+\frac{\sigma}{2}=\pi \quad (6)$$

Observing (6), the control variable of the conduction angle σ of the TCR corresponding to the control variable of the triggering delay angle α which is between $\pi/2$ and π will be between π and zero. The Laplace transformation of the output signal $E_c(s)$ of the PI controller is indicated by,

$$E_c(s)=\left(K_P+\frac{K_I}{s}\right)\left(V_{ref}(s)-V_{tr}(s)\right) \quad (7)$$

where $V_{ref}(s)$, $V_{tr}(s)$ are the Laplace transformation of the reference voltage and the rectified voltage proportional to the terminal voltage of the three-phase SEIG, respectively, K_P and K_I are the Proportional gain and Integral gain of the PI controller, respectively. The above equation can be expressed in the discrete form as follow,

$$\begin{aligned}E_c(k)=E_c(k-1)&+(K_p+T_sK_I)\left[V_{ref}(k)-V_{tr}(k)\right]\\&-K_P\left[V_{ref}(k-1)-V_{tr}(k-1)\right]\end{aligned} \quad (8)$$

where $[V_{ref}(k)-V_{tr}(k)]$ is the terminal voltage error signal at the sampling time k, $[V_{ref}(k-1)-V_{tr}(k-1)]$ is the terminal voltage error signal at the sampling time (k-1), T_s is the sampling period(sec).

5. Steady-State and Operating Performances of Three-Phase SEIG Excited By SVC

5.1 Equivalent Circuit Analysis

The three-phase SEIG equivalent circuit [2-5] is depicted in Fig.5. The equivalent susceptance $B_{TCR}(\sigma)$ of the TCR and the capacitive reactance X_{TSC} of the TSC, which is switched on under the conditions that the terminal voltage of the three-phase SEIG is less than the desired voltage(220 V) and the conduction angle $\sigma=0$ of the TCR or the triggering delay angle $\alpha=\pi$, are connected in parallel with the fixed excitation reactance X_C.

The impedance approach-based circuit analysis is applied on the approximate equivalent circuit of the three-phase SEIG excited by the SVC depicted in Fig.5 with the per-unit frequency, f ($f=F/F_b$, F and F_b are the generated output frequency and the base frequency of the three-phase SEIG) and the per-unit rotor speed υ($\upsilon=N/Ns$) as state variables. The squirrel cage rotor current I_2 referred to the stator winding side of the three-phase SEIG can be defined as,

$$I_2=\frac{E_1}{R_2\sqrt{\dfrac{1}{(f-\upsilon)^2}+\left(\dfrac{X_2}{R_2}\right)^2}} \quad (9)$$

The term $(f-\upsilon)$ is extremely small from a practical point of view. As a result, the term (X_2^2/R_2^2) could be substantially neglected with respect to $[1/(f-\upsilon)^2]$.

Therefore, the above equation of the rotor current I_2

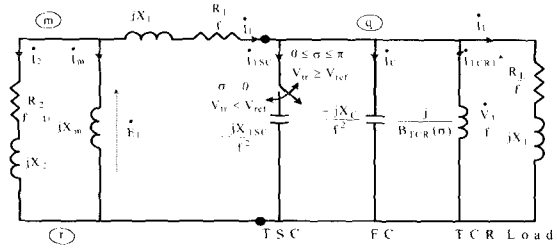

Fig. 5. Per-phase approximate equivalent circuit of three-phase SEIG excited by SVC(FC,TCR & TSC).

referred to the stator circuit side can be expressed by the following equation,

$$I_2 = \frac{(f-\upsilon)E_1}{R_2} \tag{10}$$

The mechanical input power P_i of the three-phase SEIG is defined as[1]-[2],

$$P_i = -3I_2^2 \frac{R_2}{(f-\upsilon)}(\frac{\upsilon}{f}) \tag{11}$$

By substituting I_2 in (10) into (11) and making a mechanical power balance through equating (1) to (11), the per-unit speed; υ is expressed as a function of the per-unit frequency f as follows,

$$\upsilon = \frac{(\tau_0 + \frac{3E_1^2}{R_2\omega_s})f}{\upsilon_0 f + \frac{3E_1^2}{R_2\omega_s}} \tag{12}$$

By employing the impedance approach analysis in Fig. 5, the following equation can be easily written by,

$$(\dot{Z}_{rm} + \dot{Z}_{mq} + \dot{Z}_{qr})\dot{I}_1 = 0 \tag{13}$$

$\dot{I}_1$ does not equal to zero for the self-excitation power generation mode and the successful generated terminal voltage building up of the three-phase SEIG, the following impedance relationship is held ,

$$\dot{Z}_{rm} + \dot{Z}_{mq} + \dot{Z}_{qr} = 0 \tag{14}$$

where $\dot{Z}_{rm}$, $\dot{Z}_{mq}$ and $\dot{Z}_{qr}$ can be described by considering the equivalent circuit shown in Fig. 5 and defined as (A1), (A2) and (A3), respectively in Appendix.

For a given fixed excitation capacitive reactance X_C, a TSC capacitive reactance X_{TSC}, a TCR inductive susceptance $B_{TCR}(\sigma)$, a load resistance R_L and a load reactance X_L, the three-phase SEIG machine parameters of its stator and rotor; R_1, X_1 , R_2 and X_2 and the torque-speed characteristics of the VSPM (τ_o and υ_o), the two non-linear simultaneous equations of the magnetizing reactance X_m, as a function of the per-unit frequency f, can be derived by equating the imaginary and real parts of (14) to zero and arranged as follows,

$$X_m = -\frac{C_0 + C_1 f + C_2 f^2 + C_3 f^3 + C_4 f^4 + C_5 f^5}{A_0 + A_1 f + A_2 f^2 + A_3 f^3 + A_4 f^4 + A_5 f^5} \tag{15}$$

$$X_m = \frac{D_0 + D_1 f + D_2 f^2 + D_3 f^3 + D_4 f^4 + D_5 f^5}{(B_0 + B_1 f + B_2 f^2 + B_3 f^3)f^2} \tag{16}$$

Equating the right-hand side of (15) and (16) and then mixing cross-multiplication of the successive terms yields the 10^{th} order polynomial equation written by,

$$\begin{aligned} &Y_{10}f^{10} + Y_9 f^9 + Y_8 f^8 + Y_7 f^7 \\ &+ Y_6 f^6 + Y_5 f^5 + Y_4 f^4 + Y_3 f^3 \\ &+ Y_2 f^2 + Y_1 f + Y_0 = 0 \end{aligned} \tag{17}$$

where the real coefficients from Y_0 to Y_{10} have been systematically expressed in terms of the constants A_i(i=0~5), B_j(j=0~3), C_k(k=0~5) and D_l(l=0~5) and indicated in Appendix.

5.2 Operating Characteristics

From (17), the per-unit frequency f can be determined by using the Newton Raphson method and then substitute the per-unit frequency f into (15) or (16) to calculate the magnetizing reactance X_m. The air gap voltage E_1 is evaluated from the magnetization characteristic defined by the relationship between the air gap voltage E_1 and the magnetizing reactance X_m. To determine the magnetization curve of the three-phase SEIG, the three-phase induction machine is driven at the rated synchronous speed Ns =1500 rpm and a three-phase variable voltage as an ac supply is connected to the stator winding at the rated frequency 50Hz[1]-[16]. According to the above conditions, the slip of the three-phase induction machine equals to zero and hence the rotor branch in Fig.

5 is equivalently opened. Therefore, the magnetizing reactance X_m is estimated by using the equivalent circuit shown in Fig. 5 without the fixed excitation capacitive reactance X_C, the TSC capacitive reactance X_{TSC}, the TCR inductive susceptance $B_{TCR}(\sigma)$ and the load impedance as follow,

$$X_m = \sqrt{(\frac{V_s}{I_S})^2 - (R_1)^2} - X_1 \tag{18}$$

where the experimental data of the per-phase supply voltage V_s and the current I_s is indicated in Fig.6. The air gap voltage E_1 is then calculated by,

$$E_1 = X_m I_s \tag{19}$$

The relation between the air gap voltage E_1 and the magnetizing reactance X_m is obtained experimentally and depicted in Fig. 7. To evaluate the three-phase SEIG characteristics, the magnetization curve obtained experimentally is represented with a piece-wise linear characteristics by the following equation giving a sufficiently good mapping of the air gap voltage E_1 versus the magnetizing reactance X_m nonlinear curve as shown in Fig. 7. Using a piece-wise linear representation the air gap voltage E_1 is given by,

$$E_1 = \begin{cases} 207.2 - 3.77X_m & X_m \le 24.2 \\ 541.7 - 17.79X_m & 24.2 \le X_m \le 26.5 \\ 0 & X_m \ge 26.5 \end{cases} \tag{20}$$

For estimating the three-phase SEIG performances, the following equations are derived by using the per-phase equivalent circuit of the three-phase SEIG excited by the SVC shown in Fig. 5,

$$I_1 = E_1 \frac{\sqrt{R_2^2 + (f-\upsilon)^2 (X_2 + X_m)^2}}{X_m \sqrt{R_2^2 + (f-\upsilon)^2 X_2^2}} \tag{21}$$

$$I_L = I_1 \frac{X_{SVC}}{\sqrt{\frac{R_L^2}{f^2} + (X_L - X_{SVC})^2}} \tag{22}$$

$$V_t = I_L \sqrt{R_L^2 + (fX_L)^2} \tag{23}$$

$$P_L = 3I_L^2 R_L \tag{24}$$

$$Q_L = 3I_L^2 (fX_L) \tag{25}$$

where, $X_{SVC} = \dfrac{X_C + X_{TSC}}{f^2 - (X_C + X_{TSC}) B_{TCR}(\sigma)}$.

I_1, V_t, I_L, P_L and Q_L are the per-phase stator current, the per-phase generated terminal voltage of the three-phase SEIG excited by a SVC and driven by a VSPM, the per-phase load current, and the total active power and reactive power of the balanced load, respectively.

6. Simulation and Experimental Results

6.1 Operating Performance Evaluations

The steady-state analytical algorithm of the three-phase SEIG driven by a VSPM is based on its per-phase equivalent circuit shown in Fig. 5 with neglecting the per-phase equivalent inductive susceptance $B_{TCR}(\sigma)$ of the TCR and the TSC capacitive reactance X_{TSC}. The impedance approach is applied to determine the characteristics of the three-phase SEIG driven by a VSPM as wind turbine. A feasible prototype of the three-phase SEIG driven directly by a VSPM represented by a controllable separately-excited dc motor is built and tested actually. The no-load generated terminal voltage vs. the excitation capacitance, which are selected to be chosen above the minimum value required to build up the terminal voltage of the three-phase SEIG driven by a VSPM is shown in Fig. 8. The terminal voltage of the three-phase SEIG driven by a VSPM with a certain torque-speed characteristic (τ_0=120, υ_0=133) increases with the excitation capacitance and also with changing the torque-speed characteristic from (τ_0=120, υ_0=133) to another one with the torque-speed coefficients (τ_0=110, υ_0=112) as illustrated in Fig. 4. Fig. 9 indicates the variations of the output frequency of the three-phase SEIG driven by a VSPM against its excitation capacitance at no load with different torque-speed characteristics. The output frequency of the three-phase SEIG decreases with increasing the excitation capacitance from 150 μF to 350μF at a certain torque-speed coefficients (τ_0=120, μF at

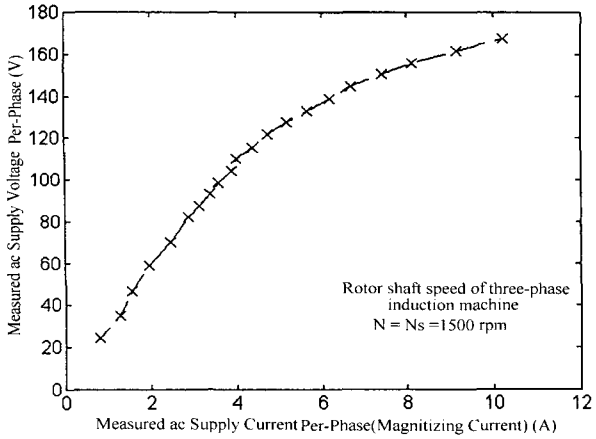

Fig. 6. Supply voltage against supply current per-phase of three- phase induction machine.

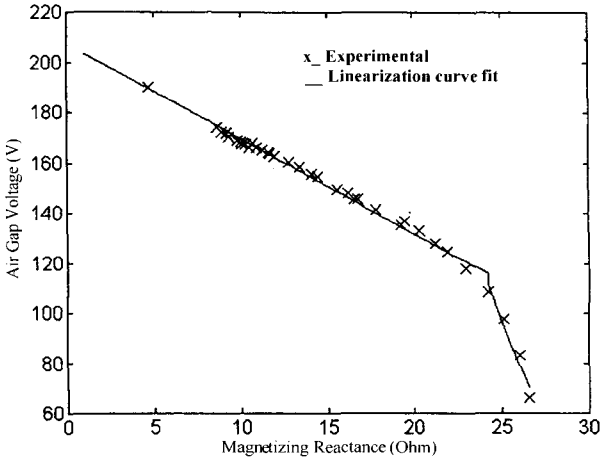

Fig. 7. Air-gap voltage vs. magnetizing reactance of SEIG.

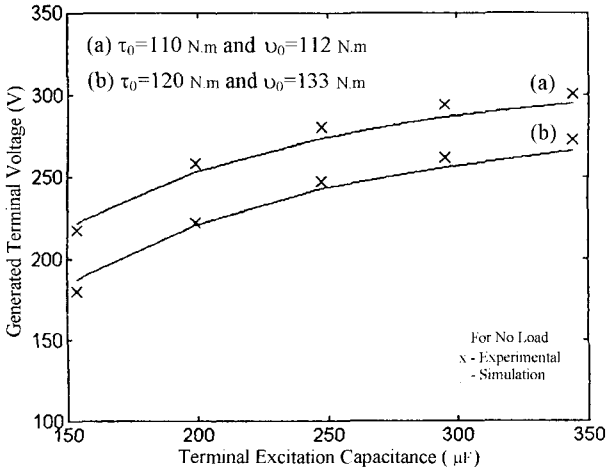

Fig. 8. No load terminal voltage variations of SEIG vs. excitation capacitance.

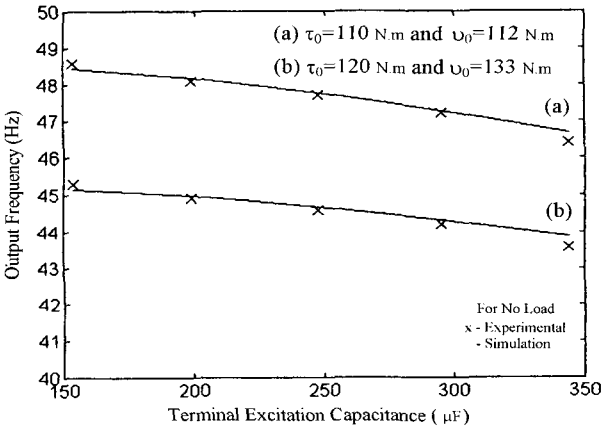

Fig. 9. Output frequency variations of SEIG vs. excitation capacitance.

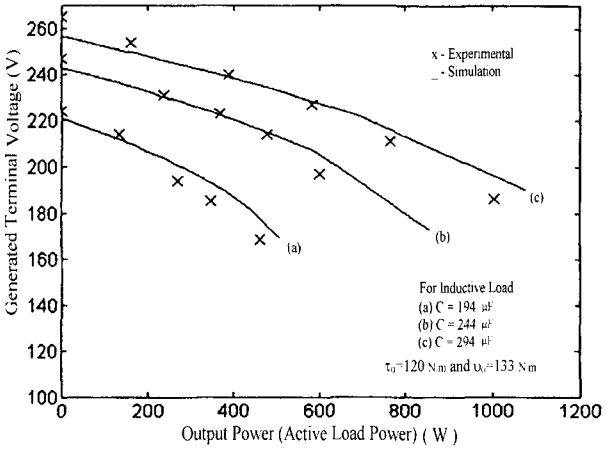

Fig. 10. Terminal voltage variations of SEIG loaded by a 0.8 lagging power factor load.

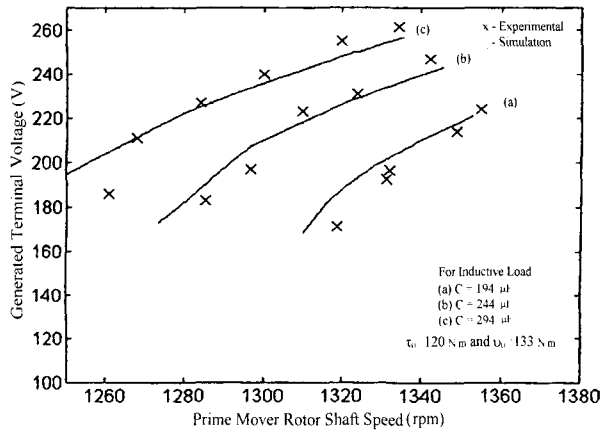

Fig. 11. Terminal voltage of SEIG against its rotor speed due to the inductive load power variations.

a certain torque-speed coefficients (τ_0=120, υ_0=133 where the VSPM speed decreases in accordance with the torque-speed characteristic of the VSPM shown in Fig. 4) and increases linearly with increasing the speed as with other torque-speed coefficients (τ_0=110, υ_0=112).

For an inductive load with 0.8 lagging power factor, specified torque-speed coefficients (τ_0=120, υ_0=133) and various capacitances (C=194 μF, 244 μF, and 294 μF per phase), Fig. 10 illustrates the induction generator terminal voltage variations with the inductive load power calculated from the digital simulation and experimental results. While Fig. 11 represents the VSPM speed variations due to the inductive load power changes vs. the terminal voltage of the three-phase SEIG. Fig. 10 and Fig. 11 indicate that the terminal voltage decreases as increasing the inductive load power, and the prime mover speed decreases in accordance with the torque-speed characteristic of the VSPM from the no load rotor speed N=1360 rpm to the full load rotor speed N=1240 rpm.

6.2 Reference Voltage Variations

The reference voltage variations are applied to test and verify the PI closed-loop feedback terminal voltage regulation of the three-phase SEIG coupled by a VSPM and supplied an inductive load using the three-phase SVC with the designed PI controller parameters. The simulation and experimental results of the generated terminal voltage response of the three-phase SEIG driven by a VSPM and excited by SVC with the reference voltage variations are depicted in Fig. 12 and Fig. 13, respectively. The simple PI control-based SVC for the voltage regulation of the three-phase SEIG driven by the VSPM proves its feasible utilization and ability for stabilizing and regulating smoothly the three-phase SEIG terminal voltage.

6.3 SEIG voltage regulation discussions

As mentioned and proved above, the terminal voltage of the three-phase SEIG is unregulated and changed due to the prime mover speed changes and the inductive load variations. The SVC-based voltage regulation scheme connected to the terminal ports of the three-phase SEIG driven by a VSPM with a certain torque-speed characteristic (τ_0=120, υ_0=133) is applied to regulate and stabilize its terminal voltage.

With fixed excitation capacitance (C=244μF per-phase) connected in parallel with the TCR, Fig. 14 shows the sim

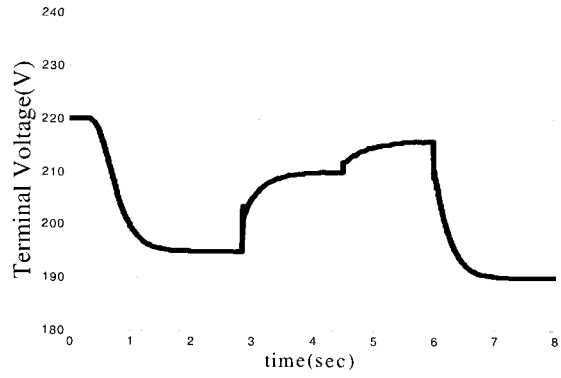

(a) Generated terminal voltage response of SEIG

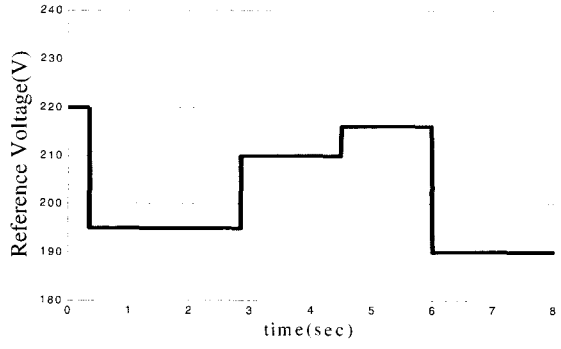

(b) Reference voltage variations response of SEIG

Fig. 12. Three-phase SEIG digital simulation terminal voltage and reference voltage responses.

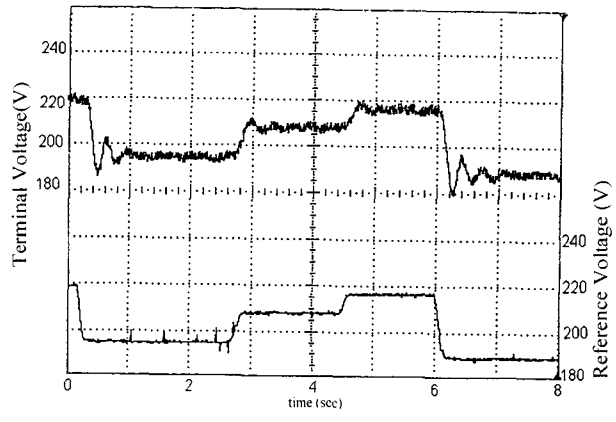

Fig. 13. Three-phase SEIG experimental terminal voltage and reference voltage responses.

-ulation results of the three-phase SEIG terminal voltage response and the thyristor triggering delay angle α of the TCR due to the inductive load variations with 0.8 lagging power factor. The load impedance components have been

increased from (R_L=90 Ohm and X_L=68 Ohm, i.e. less than the full load) to (R_L=1000 Ohm and X_L=750 Ohm, i.e. no load) and then decreased its components values from (R_L=1000 Ohm and X_L=750 Ohm) to (R_L=100 Ohm and X_L=75 Ohm). With an additional capacitor TSC required for the full load operation, Fig. 15 illustrates the simulation results of three-phase SEIG terminal voltage response and thyristor triggering delay angle α of the TCR due to the inductive load variations with 0.8 lagging power factor under the conditions of decreasing its components values from (R_L=1000 Ohm and X_L=750 Ohm) to (R_L=75 Ohm and X_L=56 Ohm). It was selected the impedance components (R_L=90 Ohm and X_L=68 Ohm) at which the terminal voltage equals to the desired voltage (220 V).

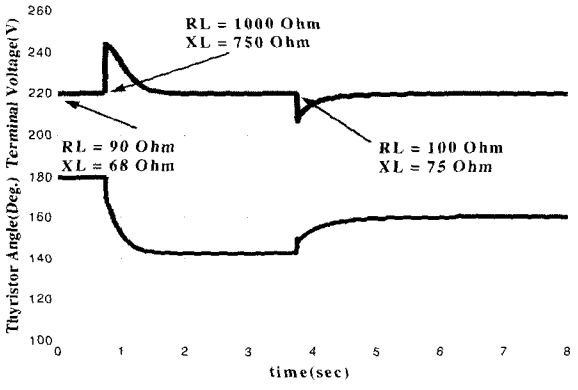

Fig. 14. Output voltage and TCR thyristor triggering angle responses using SVC composed of FC and TCR.

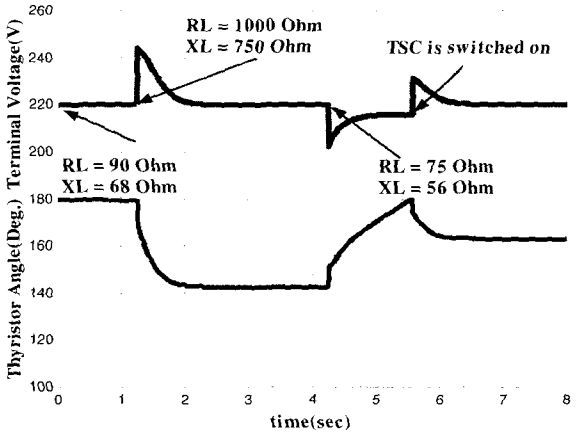

Fig. 15. Output voltage and TCR thyristor triggering angle. responses using SVC composed of FC, TSC and TCR.

To validate and test the SVC for regulating the terminal voltage of the three-phase SEIG driven by a VSPM, balanced inductive load variations with 0.8 lagging power factor are applied. Under the inductive load variations as mentioned above, Fig. 16 shows the measured three-phase SEIG terminal voltage response and the TCR trigging angle response with the SVC composed of FC and TCR. With decreasing the load impedance value until the full load operation which means that the terminal voltage is decreased lower than the reference voltage and the TCR triggering angle α equals to π. Therefore, an additional capacitance is required. The experimental responses of the three-phase SEIG terminal voltage and the TCR trigging angle with FC and TSC are represented in Fig. 17.

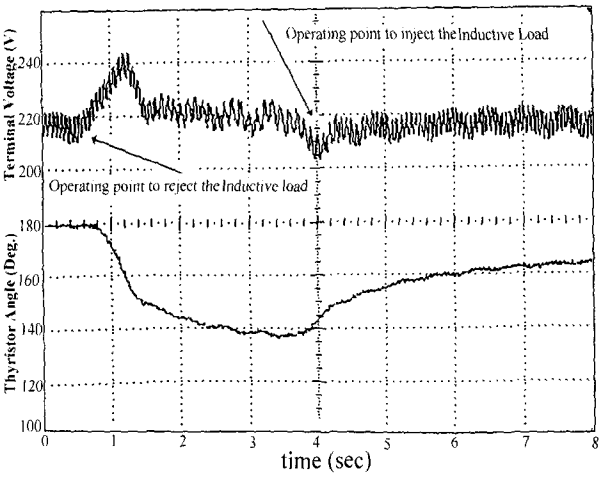

Fig. 16. SEIG experimental terminal voltage and thyristor triggering angle responses using SVC (FC and TCR).

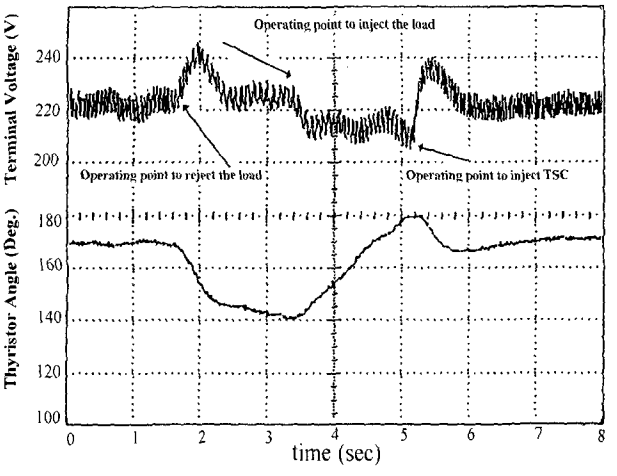

Fig. 17. SEIG experimental terminal voltage and thyristor triggering angle responses with SVC (FC, TSC & TCR).

From the above characteristic figures, the generated terminal voltage of the three-phase SEIG raises on the sudden increasing of the load parameter values; R_L and X_L. The feedback closed-loop PI controller adjusts the controlled virtual equivalent inductive susceptance B_{TCR} of the TCR by increasing its conduction angle from σ =0 which means that the TCR is off-state, i.e. decreasing the triggering delay angle α of the TCR from $\alpha=\pi$ rad. or α=180 degree. The virtual equivalent inductive susceptance value of the TCR will be increased until the generated terminal voltage of the three-phase SEIG has to be regulated to obtain the desired value or the reference value, 220V. While a sudden application or decreasing the load components of R_L and X_L values, the generated terminal effective voltage of the three-phase SEIG is decreased. The thyristor triggering delay angle α of the TCR increases to decrease the controlled equivalent inductive susceptance of the TCR regulated by the feedback closed loop-based PI controller output signal error voltage until the error voltage goes toward zero. When the full load is connected to the three-phase SEIG terminals, the thyristor triggering delay angle α of the TCR is increased until it is equal to π rad., i.e. the TCR becomes off state or σ =0. The generated terminal voltage of the three-phase SEIG is still less than the desired value (220 V). The TSC is switched on in this instant and connected to the three-phase SEIG terminals in parallel with the TCR, the generated terminal voltage of the three-phase SEIG will increase over the desired value (220 V). The PI controller in the feedback loop of the SVC-based voltage regulation adjusts the virtual equivalent inductive susceptance B_{TCR} of the TCR until the error voltage goes toward zero. The results obtained above prove that the voltage regulation of the three-phase SEIG have been carried out with fast responses.

7. Conclusions

This paper has introduced an effective algorithm for the steady-state operating performance analysis of the three-phase SEIG driven directly by the VSPM as the wind turbine. The steady-state operating performances of the three-phase SEIG have been obtained in terms of its terminal voltage in accordance with the output power and the prime-mover speed variations. In addition, this paper has dealt with the SVC for the voltage regulation of the three-phase SEIG driven by the VSPM. External variations such as the stand-alone inductive load have been applied for evaluating the proposed static VAR compensator-based PI feedback control implementation system. A three-phase SEIG prototype setup with SVC has been established for the cost effective wind turbine power conditioner used in the rural alternative energy effective utilization area from an earth environmental protection point of view. The feasible experimental curves have been validated on the practical effectiveness of the static VAR compensating control scheme.

Appendix

$$\dot{Z}_{rm} = \frac{(jX_m)\dot{Z}_r}{\dot{Z}_r + jX_m} \tag{A1}$$

$$\dot{Z}_{mq} = \frac{R_1}{f} + jX_1 \tag{A2}$$

$$\text{and } \dot{Z}_{qr} = \left(\frac{-jX_{SVC}\left(\frac{R_L}{f} + jX_L\right)}{\frac{R_L}{f} + j(X_L - X_{SVC})}\right. \tag{A3}$$

$$\text{where, } X_{SVC} = \frac{X_C + X_{TSC}}{f^2 - (X_C + X_{TSC})B_{TCR}} \tag{A4}$$

$$\dot{Z}_r = \frac{R_2}{f - \upsilon} + jX_2 \tag{A5}$$

$$= \frac{\left(\frac{3E_1^2}{\omega_s} + \upsilon_0 R_2 f\right) + j(-\tau_0 + \upsilon_0 f)X_2 f}{(-\tau_0 + \upsilon_0 f)f}$$

$$\text{or } \dot{Z}_r = \frac{(G_0 + G_1 f) + j(G_2 + G_3 f)X_2 f}{(G_2 + G_3 f)f}$$

where $G_0=3E_1^2/\omega_s$, $G_1=\upsilon_0 R_2$, $G_2=-\tau_0$ and $G_3=\upsilon_0$ τ_0=120, υ_0=133 and N_s=1500 rpm

Let $\dot{Z}_{rmeq} = \dot{Z}_{qr} + \dot{Z}_{mq}$

$$\dot{Z}_{rmeq} = \frac{R_1}{f} + jX_1 + \left(\frac{-jX_{SCV}\left(\frac{R_L}{f} + jX_L\right)}{\frac{R_L}{f} + j(X_L - X_{SCV})}\right) \qquad (A6)$$

$$\dot{Z}_{rmeq} = \frac{(F_0 + F_2 f^2 + F_4 f^4) + j(T_0 + T_2 f^2)f}{(R_L f^3 - R_L X_{CE} B_{TCR} f) + j(X_L f^3 - X_L X_{CE} B_{TCR} f - X_{CE} f)}$$

where, $X_{CE}=X_C+X_{TSC}$, $B_{TCR}(\sigma)=B_{TCR}=[\sigma-\sin(\sigma)]/\pi X_{TCR}$

$F_0=-R_LR_1X_{CE}B_{TCR}$, $F_2=R_LR_1+(X_1X_LB_{TCR}+X_1+X_L)X_{CE}$,
$F_4=-X_LX_1$, $T_0=-X_{CE}(R_L+R_1+R_LX_LB_{TCR}+R_1X_LB_{TCR})$,
$T_2=R_1X_L+R_LX_1$,
$C_0=G_0T_0+G_2X_2F_0$,
$C_1=G_1T_0+G_3X_2F_0$,
$C_2=G_0T_2+G_2X_2F_2$,
$C_3=G_1T_2+G_3X_2F_2$,
$C_4=G_2X_2F_4$,
$C_5=G_3X_2F_4$,
$A_0=-G_0R_L X_{CE} B_{TCR}+G_2F_0$,
$A_1=-G_1R_L X_{CE} B_{TCR}+G_3F_0$,
$A_2=G_2X_2 X_{CE}(X_LB_{TCR}+1)+G_0R_L+G_2F_2$,
$A_3=G_3X_2 X_{CE}(X_LB_{TCR}+1)+G_1R_L+G_3F_2$,
$A_4=-G_2X_2X_L+G_2F_4$,
$A_5=-G_3X_2X_L+G_3F_4$,
$D_0=G_0F_0$, $D_1=G_1F_0$,
$D_2=G_0F_2-G_2X_2T_0$,
$D_3=G_1F_2-G_3X_2T_0$,
$D_4=G_0F_4-G_2X_2T_2$,
$D_5=G_1F_4-G_3X_2T_2$,
$B_0=G_2(T_0-R_LX_2X_{CE}B_{TCR})-G_0X_{CE}(X_LB_{TCR}+1)$,
$B_1=G_3(T_0-R_LX_2X_{CE}B_{TCR})-G_1X_{CE}(X_LB_{TCR}+1)$,
$B_2=G_2(T_2+R_LX_2)+G_0X_L$,
$B_3=G_3(T_2+R_LX_2)+G_1X_L$,
$Y_0=A_0D_0$,
$Y_1=A_0D_1+A_1D_0$,
$Y_2=A_0D_2+A_1D_1+A_2D_0+B_0C_0$,
$Y_3=A_0D_3+A_1D_2+A_2D_1+A_3D_0+B_0C_1+B_1C_0$,
$Y_4=A_0D_4+A_1D_3+A_2D_2+A_3D_1+A_4D_0+B_0C_2+B_1C_1+B_2C_0$,
$Y_5=A_0D_5+A_1D_4+A_2D_3+A_3D_2+A_4D_1+A_5D_0+B_0C_3+B_1C_2+B_2C_1+B_3C_0$,
$Y_6=A_1D_5+A_2D_4+A_3D_3+A_4D_2+A_5D_1+B_0C_4+B_1C_3+B_2C_2+B_3C_1$,
$Y_7=A_2D_5+A_3D_4+A_4D_3+A_5D_2+B_0C_5+B_1C_4+B_2C_3+B_3C_2$,
$Y_8=A_3D_5+A_4D_4+A_5D_3+B_1C_5+B_2C_4+B_3C_3$,
$Y_9=A_4D_5+A_5D_4+B_2C_5+B_3C_4$,
$Y_{10}=A_5D_5+B_3C_5$,

References

[1] S.Rajakarvna and R.Bonert, "A Technique for The Steady state Analysis of Self-Excited Induction Generator with Variable Speed", *IEEE Trans. on Energy Conversion*, Vol. 10, No. 1, pp. 10-16, Mar. 1995.

[2] Tarek Ahmed, M.Z.El-Sadek and G.El-Saady, "On Line Simulation of Wind Turbine by Separately Excited DC Motor Driving Self-Excited Induction Generator", MEPCON'98, 6th International Middle East Power Systems Conference, pp. 105-109, 1998.

[3] IEEE Special Stability Controls Working Group Report, "Static VAR Compensator Models for Power Flow and Dynamic Performance Simulation", *IEEE Transactions on Power Systems*, Vol. 9, No. 1, Feb. 1994.

[4] Lahcene Quazene and George McPherson "Analysis of The Isolated Induction Generator", *IEEE Trans. on Power Apparatus and Systems*, Vol. PAS-102, No. 8, pp. 2793 -2798, Aug. 1983.

[5] N.H.Malik and S.E.Haque "Steady-state Analysis and Performance of An Isolated Self-Excited Induction Generator", *IEEE Trans. on Energy Conversion*, Vol. EC-1, No. 3 pp. 134-139, Sep. 1986.

[6] A.K.Aljabri and A.I.Alolah, "Capacitance Requirement for Isolated Self-Excited Induction Generator", *IEE Proceedings*, part B, Vol. 137, No. 3, pp. 154-159, May. 1990.

[7] T.F.Chan, "Analysis of A Single-Phase Self-Excited Induction Generator", *Electric Machine and Power Systems*, Vol. 23, pp. 149-162, 1995.

[8] Ermis, H.B.Erton, M.Demirekler, B.M.Saribatir, Y.Uctvg, M.E.Sezer and I.Cadirici, "Various Induction Generator Schemes for Wind-Electricity Generation", *Electric Power Systems Research*, Vol. 23, pp. 71-83, 1992

[9] L.Shridhar, B.P.Singh and C.S.Jha, "A Step Towards Improvements in The Characteristics of Self-Excited Induction Generator", *IEEE Trans. On Energy Conversion*, Vol. 8, No. 1, pp. 40-46, Mar. 1993.

[10] T.F.Chan, "Capacitance Requirements of Self-Excited Induction Generators", *IEEE Trans. on Energy Conversion*, Vol. 8, No. 2, PP. 304-311, June. 1993.

[11] S.P.Singh, M.P.Jain and Bhim Singh, "A New Technique for Analysis of Self-Excited Induction Generator", Electric Machine and Power Systems, Vol. 23, pp. 647-656, 1995.

[12] Li Wang and Lian-Yi Su, "Effects of Long-Shunt and Short-Shunt Connections on Voltage Variations of A

Self-Excited Induction Generator", *IEEE Trans. on Energy Conversion*, Vol. 12, No. 4, pp. 368-374, Dec. 1997.

[13] W. Koczara, "Variable Speed Three-Phase Power Generation Set", EPE-2001, 2001.

[14] A. Koyanagi "Maximum Power Point Tracking of Wind Turbine Generator Using a Flywheel", Proceedings of the 2001 Japan Industry Application society Conference, Vol. 1, pp. 395-398, 2001.

[15] Tarek Ahmed, Osamu Noro, Koji Sato, Eiji Hiraki and Mutsuo Nakaoka "Single-Phase Self-Excited Induction Generator with Static VAR Compensator Voltage Regulation for Simple and Low Cost Stand-Alone Renewable Energy Utilizations Part I: Analytical Study" *KIEE International Transactions on Power Engineering*, Vol. 3-A, No. 1, pp. 17-26, 2003.

[16] Tarek Ahmed, Osamu Noro, Koji Sato, Eiji Hiraki and Mutsuo Nakaoka "Single-Phase Self-Excited Induction Generator with Static VAR Compensator Voltage Regulation for Simple and Low Cost Stand-Alone Renewable Energy Utilizations Part II: Simulation and Experimental Results" *KIEE International Transactions on Power Engineering*, Vol. 3-A, No. 1, pp. 27-34, 2003.

Tarek Ahmed received his M.Sc. degree in electrical engineering from the Electrical Engineering Department, Faculty of Engineering, Assiut Univer sity, Egypt in 1998. He is working a staff member as an assistant lecturer in the Electrical Engineering Department, Faculty of Engineering, Assiut University, Assiut, Egypt. He is currently a Ph. D. candidate student with the Power Electronic System and Control Engineering Laboratory, the Division of Electrical and Electronic Systems Engineering, the Graduate School of Science and Engineering, Yamaguchi University, Yamaguchi, Japan. He has received the Paper Award from the Institute of Electrical Engineers of Japan (IEE-J) in 2003. His research interests are in the new applications of the advanced high frequency resonant circuits and systems with the renewable energy related soft switching PWM rectifier and sinewave PWM inverter power conditioner. Mr. Ahmed is a student-member of the Institute of Electrical and Electronics Engineers of USA (IEEE-USA), the Institute of Electrical Engineering and Installation of Engineers (IEIE-Japan), the Institute of Electrical Engineers (IEE-Japan) and Japan Institute of Power Electronics (JIPE).

Katsumi Nishida received the B.S., and M.S. degrees in electrical engineering from the Tokyo Institute of Technology, Tokyo in 1976, 1978, respectively. He received the Ph.D. degree from the Division of Electrical and Electronic Systems Enginee ring, the Graduate School of Science and Engineering, Yamaguchi University, Yamaguchi, Japan in 2002. He is engaged in research on the power factor correction of the PWM converter and the current control of the three-phase active power filter with the dead-beat technique and the adaptive signal processing technique. Dr.-Eng. Nishida is a member of the Institute of Electrical and Electronics Engineers of USA (IEEE-USA), the Institute of Electrical Engineers of Japan (IEE-Japan) and Japan Institute of Power Electronics (JIPE).

Mutsuo Nakaoka received his Dr.-Eng. degree in Electrical Engin eering from Osaka University, Osaka, Japan in 1981. He joined the Electrical and Electronics Engineering Department of Kobe University, Kobe, Japan in 1981 and served as a professor of the Depart ment of Electrical and Electronics Engineering, the Graduate School of Engineering, Kobe University, Kobe, Japan. until 1995. Now he is working a professor in the Electrical and Electronics Engineering Department, the Graduate School of Science and Engineering, Yamaguchi University, Yamaguchi, Japan. His research interests include application developments of power electronics circuits and systems. He has received more than ten Awards such as the 2001 premium prize paper award from IEE-UK, the 2001 and 2003Best Paper Award from IEEE -IECON, the 2000 third paper award from IEEE-PEDS, 2003 James Melcher Prize Paper award from IEEE-IAS. He is now a chairman of IEEE Industrial Electronics Society Japan Chapter.

Prof. Dr.-Eng. Nakaoka is a member of the Institute of Electrical Engineering Engineers of Japan, Institute of Electronics, Information and Communication Engineers of Japan, Institute of Illumination Engineering of Japan, European Power Electronics Association, Japan Institute of Power Electronics, Japan Society of the Solar Energy, Korean Institute of Power Electronics, IEE-Korea and IEEE.